

Fourier analysis of Fe I lines in the spectra of the Sun, α Centauri A, Procyon, Arcturus, and Canopus

V.A. Sheminova and A. S. Gadun

Main Astronomical Observatory, National Academy of Sciences of Ukraine
Zabolotnoho 27, 03689 Kyiv, Ukraine
E-mail: shem@mao.kiev.ua

Abstract

We used spectral observations of Fe I line profiles with a 200 000 resolution to determine micro and macroturbulent velocities in the atmospheres of the Sun as a star, α Cen A, Procyon (α CMi), Arcturus (α Boo), and Canopus (α Car). Isotropic microturbulent velocities (V_{mi}) and radial-tangential macroturbulent velocities (V_{ma}^{RT}) were found to be a quite suitable approximation to the velocity field in the atmospheres of all stars studied except Canopus. The average velocities V_{mi} and V_{ma}^{RT} are 0.8 ± 0.1 and 2.6 ± 0.3 km/s for the Sun as a star, 0.8 ± 0.2 and 2.9 ± 0.4 km/s for α Cen A, 0.8 ± 0.3 and 5.9 ± 0.2 km/s for Procyon, 1.0 ± 0.2 and 4.6 ± 0.3 km/s for Arcturus. The velocity field in the atmosphere of Canopus can be described by an anisotropic radial-tangential distribution of microturbulence with $V_{mi}^{RT} = 2.1$ km/s and anisotropic distribution of macroturbulence with $V_{ma}^{rad} = 17 \pm 2$ km/s and $V_{ma}^{tan} = 1.3 \pm 1.0$ km/s. From Fourier analysis of broadening and shapes of three spectral lines of Fe I, we have derived the rotation velocity $V_e \sin i = 3.5 \pm 0.2$ km/s for Canopus.

1 Introduction

An advantage of the Fourier analysis of stellar spectra is that it allows the separation of the contributions to the Fourier transforms from various processes which are responsible for line broadening. Some examples of application of the Fourier analysis to the investigations of stellar rotation and astrospectroscopic turbulence as well as the description of its details and problems can be found in Gray's book [18]. However, it is not always possible to realize all the advantages of this technique in actual practice, as the Fourier transforms of the principal broadening processes are reliably separated in the high frequency domain, which can be studied only in observations with high signal-to-noise ratios and high spectral resolutions. Nevertheless, the Fourier analysis extended the possibilities for interpreting the broadening of spectral lines produced by mechanical motions in stellar atmospheres. While it was found for solar type stars that line broadening and shifts are caused by the photospheric overshooting convection and oscillatory motions [2, 11, 38, 39], the question of the nature of motions in the atmospheres of nonsolar type stars remains open [6, 9, 26].

Our analysis is based on unique spectral observations made by Dravins [8], and its main objective is to determine the rotation velocity and study the distribution of micro-macroturbulent

velocities in the atmospheres of stars of various types. With the stars appropriately selected, we are able to solve the following problems.

1. Follow variations in the velocity field when going from the Sun to other stars in the H–R diagram. The Sun can be used as a test star.

2. Models are available for all stars studied. They are either theoretical three-dimensional (3D) inhomogeneous models (the Sun and Procyon [2, 38, 39], α Cen A [39]) or semiempirical multicomponent models (Arcturus and Canopus [9]). Thus the analysis results can be interpreted more or less reliably and used to explain the granulation boundary in the H–R diagram found by Gray and Nagel [24]. Lines in the spectra of the stars located to the right of this boundary (cooler stars) have a red C-shaped asymmetry of the solar type, while lines in hotter stars display a violet inversion asymmetry. The position of the boundary approximately corresponds to those stars of luminosity classes III–V in which convective envelopes adjacent to atmospheric layers can already form. Thus, a red asymmetry of spectral lines may suggest that granulation exists on the stellar surface and the velocity field of the thermal convection (or photospheric overshooting convection) strongly affects the line profiles. This conclusion is at variance, however, with the data for stars of luminosity classes I–II, for which Gray’s granulation boundary and the boundary of convection-induced envelopes (according to the mixing-length theory [24]) do not coincide. At the same time a violet asymmetry of stellar spectral lines may be interpreted as a prevalence of mechanical motions other than convection in stellar atmospheres (oscillations, mass loss, etc.).

3. Four stars in our list (the Sun, α Cen A, Procyon, Arcturus) have convective envelopes. The photospheric overshooting convection is of different character in each star, however, and it is of interest to relate the distinctions to the astrospectroscopic turbulence parameters. The fifth star, the supergiant Canopus, lies to the left of the granulation boundary, it has no convective envelope, and the lines in its spectrum have a violet inversion asymmetry [8]. Analysis of its atmospheric velocity field is of special interest.

2 Observations

We used the spectrograms acquired by Dravins [8] at the European Southern Observatory in 1982–1984. A double-pass coude echelle spectrometer provided a 200 000 resolution at a dispersion of 1 pm/mm. The instrumental profile is nearly Gaussian in shape with the FWHM equal to 2.3 km/s. The Nyquist frequency of observations is on $\sigma_N \approx 0.84$ s/km. The first zero of the Fourier transform of the instrumental profile lies at the frequency $\sigma \approx 0.32$ s/km. The S/N ratio exceeds 300.

Table 1: Basic parameters of the stars studied

Star	Sp	T_{eff} , K	$\log g$	m_*/m_\odot	M_v	$V_e \sin i$, km/s	A_{Fe}^{mod}
Sun	G2 V	5770 [1]	4.44 [1]	1.00	4.38 [1]	1.85 [5]	7.55
α Cen A	G2 V	5770 [3]	4.29 [13]	1.08 [7]	4.38 [7]	1.8 [11]	7.55
Procyon	F5 IV–V	6500 [45]	4.04 [45]	1.76 [45]	2.66 [45]	2.9 [11]	7.55
Arcturus	K1 III	4260 [36]	0.90 [36]	0.60 [36]	-0.23 [36]	2.4 [21]	6.94 [36]
Canopus	F0 II	7350 [40]	1.80 [40]	8.00 [34]	-4.70 [1]	3.5 This study	7.55

The principal characteristics of the stars studied were taken, for the most part, from paper [13]. Table 1 gives the effective temperature T_{eff} , gravitational acceleration $\log g$, relative mass m_*/m_\odot , absolute luminosity M_v , rotation velocity $V_e \sin i$, and iron abundance adopted in the models A_{Fe}^{mod} . The lines selected for the analysis were unblended or had one unblended wing.

The profiles were not smoothed lest additional distortions appear in the Fourier transforms. First the observed profiles were interpolated with a step which varied from line to line within the range 0.001–0.005 nm (see below). Then the right wing referred to the local continuum was averaged with the left wing, and thus the lines were symmetrized. The line center was defined as the center of gravity of the line core, which comprised 10 percent from the minimum. When one wing had a small blend, it was corrected according to the shape of the unblended wing. As soon as the wing reached the local continuum level, the profile was completed by zeros on both sides. The length of the spectral region remained constant for all lines in this case (in view of a specially selected step of wavelength interpolation). As a result, the Fourier transform resolution was the same for all lines — $\Delta\sigma = 0.009$ s/km.

When dealing with Fourier transforms, one has always to take proper account of the noises in the observed profiles [22]. If $V_e \sin i/V_{ma} > 2$, the information about the parameters V_{ma} and $V_e \sin i$ resides almost exclusively in the amplitude of the side lobe, which is located at relatively low frequencies. These parameters are determined quite reliably. When $V_e \sin i/V_{ma} < 1$ (this is the case here), all information about V_{ma} and $V_e \sin i$ resides in the principal lobe, and this presents additional problems in separating V_{ma} , $V_e \sin i$, and V_{mi} . The situation improves when $S/N > 500$ and a side lobe formed due to saturation of the absorption line can be seen at higher frequencies in strong lines. This lobe is very sensitive to the microturbulence, and the velocity parameters can be separated more reliably. We measured noise levels for every Fourier transform of the lines at high frequencies beginning with the frequency of the first zero of the instrumental profile, where no signal from the line is observed. The average noise was -3.3 dex. This noise is superimposed on the signal beginning with the frequency $\sigma \approx 0.12$ s/km. The first zero in the transforms for our stars is found, as a rule, between frequencies of 0.13 and 0.2 s/km. Therefore the analysis of the principal lobe gives the results for any line, while the side lobe can be analyzed only for those strong lines in which the side lobe amplitude exceeds the noise level. To be able to separate the micro-macrovelocities, we selected only strong Fe I lines, with the highest S/N ratio. The equivalent widths of such lines are 10–20 pm. Table 2 gives these lines together with their parameters. The oscillator strengths found from the equivalent widths of solar lines were taken from [27] or calculated in the way described in [27].

Table 2: Line list

λ , nm	Multiplet	EPL , eV	$\log gf_w$
460.29466	39	1.48	-3.14
536.48801	1146	4.44	0.38
536.54063	786	3.57	-1.41
536.74755	1146	4.41	0.22
543.45315	15	1.01	-2.12
633.53378	62	2.20	-2.23
633.68328	816	3.69	-0.81
643.08538	62	2.18	-2.46

3 Modelling the line profiles

The LTE line profiles were calculated with the SPANSAT program [15], and the Fourier transforms of the profiles were calculated with the FFT program from [18]. The instrumental profile is taken into account more exactly by the convolution of the calculated line profile with the instrumental profile rather than excluding it from the observed profile. That is why we compare

the observed and calculated profiles and their Fourier transforms which contain the instrumental profile.

Our calculations are based on the homogeneous stellar model atmospheres constructed with Kurucz's model grid [33] with the parameters T_{eff} and $\log g$ from Table 1.

The turbulent velocity field was simulated within the concept of micro-macroturbulence. We considered three velocity distribution variants for the microturbulence.

1. Isotropic microturbulence — a Gaussian distribution with the most probable value V_{mi} . In calculations the microturbulence is taken into account by the convolution with the line absorption coefficient.
2. Nonisotropic microturbulence — every element in the radial flow has a complete set of tangential velocities, and the radial as well as the tangential velocities have Gaussian distributions. Their convolution gives a radial-tangential distribution with the dispersion $V_{mi}^2(\mu) = (V_{mi}^{rad}\mu)^2 + (V_{mi}^{tan})^2(1 - \mu^2)$, where $\mu = \cos\theta$, θ being the heliocentric angle.
3. Anisotropic microturbulence — the radial and the tangential distributions do not inter-mingle, and the turbulent flow is either radial with the area S_{mi} or tangential with the area $1 - S_{mi}$. The anisotropic microturbulence is included in the algorithm as a Voigt function in the form of a sum of two distributions: $H = H(V_{mi}^{rad}\mu)S_{mi} + H(V_{mi}^{tan}(1 - \mu^2)^{1/2})(1 - S_{mi})$.

The macroturbulence was assumed to be in the form of two distributions.

1. Isotropic macroturbulence — the star is divided into regions which contain many macroelements with a Gaussian velocity distribution and the most probable velocity V_{ma} . The macrovelocity is taken into account in this case through the convolution of the macroturbulent velocity distribution with the flux spectrum of a star with no macroturbulence in its atmosphere.
2. Anisotropic macroturbulence (or the radial-tangential model — V_{ma}^{RT}) — the radial and the tangential macroturbulence given as a sum of two Gaussians: $G = G(V_{ma}^{rad}\mu)S_{ma} + G(V_{ma}^{tan}(1 - \mu^2)^{1/2})(1 - S_{ma})$, where S_{ma} is the area fraction occupied by the radial component. In calculations the macrovelocity is taken into account through the convolution with the line profile for every position on the stellar disk.

The rotation velocity $V_e \sin i$ was taken as a constant on the assumption that the star is spherical and rotates as a solid body. The rotation was simulated by direct averaging over the star's disk. The limb darkening was allowed for directly. Position on the disk was specified by two variables — the position angle p and the angle θ between the center of the apparent disk and the direction of emerging radiation. Integration over the disk was performed with the Gauss quadrature formula with a constant weight function (for μ^2) and the quadrature formula of the highest trigonometrical precision (for p).

The classical Fourier analysis [16, 17, 19, 20, 21, 22, 23, 43] allows all three velocities (V_{mi} , V_{ma} , $V_e \sin i$) to be separated. The separation scheme, described also in [18], was realized for the analysis of lines in the spectrum of Canopus, whose rotation velocity was rarely measured before. A value of 15 km/s given in catalog [47] was derived in 1953 as a very rough estimate from half-widths of spectral lines. As to the other stars, their rotation velocities cannot be determined from the observations used by us more exactly than it was done earlier (see Table 1).

So, the special calculation scheme realized for four stars except Canopus was as follows. With known and invariable model atmosphere, rotation velocity, and damping constant (the

correction factor is unity for all stars), a thermal profile is simulated with the microturbulence, rotation velocity, and instrumental profile taken into account. Abundances and oscillator strengths are initially set as given in Tables 1 and 2. Next the Fourier transform of this simulated profile is compared to the Fourier transform of the observed profile. Varying V_{mi} , we get the best fit of the simulated first zero and side lobe to the observed ones, and the principal lobe amplitude in the simulated Fourier transform must be equal to or slightly higher than the observed amplitude. If the equivalent widths of the simulated and the observed lines are not equal, we make them coincide by varying the parameter Agf . In this way, from the coincidence of the first zero, the side lobe, and the equivalent width, we determine the microturbulent velocity V_{mi} .

At the second stage we separate the Fourier transform of the residual profile from the Fourier transform of the observed profile, the former being the Fourier transform of the macroturbulence distribution, and then we match it against a grid of Fourier transforms of macroturbulent velocity functions calculated for different distributions and dispersions. We obtain the Fourier transform of the residual profile as the result of the simple operation: $m(\sigma) = d(\sigma)/[f(\sigma)i(\sigma)g(\sigma)]$. Here we introduce the following designations for the Fourier transforms of profiles: $d(\sigma)$ for the observed profile, $f(\sigma)$ for the thermal profile with microturbulence taken into account, $i(\sigma)$ for the instrumental profile, $g(\sigma)$ for the rotation function, and $m(\sigma)$ for the macroturbulent velocity distribution. When the macroturbulent velocity is determined, the calculated and the observed central line intensities must coincide.

4 Results

We assumed the radial and tangential components to be equal in the anisotropic models (for microturbulence as well as for macroturbulence). The areas occupied by them were also assumed to be similar. Such assumptions are made usually in the Fourier analysis of line profiles in stellar spectra because the number of unknown parameters can be reduced in this case. Equality of V^{rad} and V^{tan} in nonisotropic microturbulence models results in an isotropic distribution, and so we shall not use the nonisotropic model in this study.

Table 3 gives the velocities derived for each line analyzed. Given also are the observed values of d_c and W (with the instrumental profile not subtracted) as well as the effective depths of line formation $\log \tau_5$ calculated with the depression contribution functions. One can judge from these parameters how warranted is averaging the velocities over all lines. No conclusion on velocity stratification in the stellar atmospheres can be drawn based on the depths $\log \tau_{5,W}$ derived here, since the layer in which a line is formed is much wider for the star as a whole than for a feature on the stellar disk. Besides, we do not take into consideration the velocity gradients in the atmospheres, and the number of lines used in our analysis is too small. The velocities averaged over all lines are referred to the depths of formation averaged over all lines. The values in columns 5 and 6 are the most probable velocities for the model with the isotropic microturbulence and the anisotropic macro-turbulence, in columns 7 and 8 for the anisotropic micro-macroturbulent velocities, and in columns 9 and 10 we give the values obtained in the classical way — the isotropic microturbulence was found from equivalent widths and the isotropic macroturbulence from central intensities.

The table gives also the *rms* values V_{rms} of macroturbulent velocity distributions, they can be used for reducing the most probable values V_{max} for the isotropic and anisotropic distributions of macroturbulent velocities to a common system with the aim to compare the results. Recall that $V_{rms} = V_{max}/\sqrt{2}$ for the Gaussian isotropic velocity distribution and $V_{rms} \approx V_{max}/2$ for the radial-tangential distribution [17].

Table 3: Fourier-analysis results for five stars

λ , nm	d_c	W , pm	$\log \tau_5$	V_{mi}	V_{ma}^{RT}	V_{mi}^{RT}	V_{mi}	V_{ma}	
Sun									
536.5	0.568	7.28	-1.7	0.9	2.3	1.5	2.3	0.6	1.6
536.7	0.688	14.15	-1.7	0.8	2.2	1.5	2.3	-	-
633.5	0.598	9.90	-2.3	0.8	2.8	1.5	2.8	0.5	1.9
633.6	0.582	11.34	-2.0	0.6	3.0	1.2	3.1	1.0	2.2
Average			-1.9	0.8	2.6	1.4	2.6	0.7	1.9
Error			0.2	0.1	0.3	0.1	0.3	0.2	0.3
V_{rms}					1.3		1.3		1.3
α Cen A									
536.7	0.712	16.19	-1.7	0.8	2.3	1.3	2.4	1.5	2.0
543.4	0.811	19.59	-2.8	1.1	3.5	1.5	3.2	-	-
633.5	0.618	10.86	-2.4	0.6	3.0	1.1	3.1	1.1	2.1
Average			-2.3	0.8	2.9	1.3	2.9	1.3	2.0
Error			0.4	0.2	0.4	0.1	0.3	0.2	0.0
V_{rms}					1.4		1.4		1.4
Procyon									
460.2	0.603	10.48	-2.1	1.2	6.1	1.5	6.1	1.7	4.1
536.4	0.488	10.09	-1.7	0.6	5.9	1.5	6.1	0.8	4.0
536.7	0.514	10.86	-1.7	0.5	5.6	1.5	6.1	1.6	4.1
Average			-1.8	0.8	5.9	1.5	6.1	1.4	4.1
Error			0.2	0.3	0.2	0.0	0.0	0.4	0.0
V_{rms}					2.9		3.1		2.9
Arcturus									
536.4	0.707	13.17	-1.8	1.4	4.9	2.0	4.9	1.4	3.4
536.5	0.671	11.30	-1.6	1.0	4.7	1.5	4.8	1.6	3.2
536.7	0.727	13.60	-1.7	0.7	4.1	1.7	4.5	1.7	3.2
Average			-1.7	1.0	4.6	1.7	4.7	1.6	3.3
Error			0.1	0.2	0.3	0.2	0.2	0.1	0.1
V_{rms}					2.3		2.4		2.3
Canopus									
536.4	0.384	7.45	-1.4	-	-	2.1	15–0.5	1.2	4.4
536.7	0.426	9.00	-1.6	-	-	2.1	16–0.5	2.1	4.5
643.0	0.210	4.95	-1.3	-	-	2.1	20–3.0	-	-
Average			-1.4			2.1	17–1.3	1.6	4.4
Error			0.1			0.0	2–1.0	0.4	0.0
V_{rms}							8–0.5		3.1

It follows from the comparison of the Fourier transforms of the observed and calculated line profiles that both microturbulence models (isotropic and anisotropic) give the same results for the Sun and α Cen A (Fig. 1). The Fourier transforms for these stars are more sensitive to macroturbulent velocity distributions. Their side lobes display some differences for the isotropic and anisotropic macroturbulence, and we may conclude that the anisotropic macroturbulence model gives a better result. For the atmospheres of Procyon and Arcturus (Fig. 1), the isotropic microturbulence describes line profiles better than the anisotropic one. The distribution of macroturbulent velocities remains anisotropic.

Selection of velocity field parameters for Canopus turned out to be a difficult task. This is so for microturbulent velocities because the lines in the spectrum of this hot star are weak and their Fourier transforms have smaller amplitudes. Besides, the line profiles differ from the profiles in other stars in that the ratio between wing width and core height is larger: the lines in Canopus have narrow cores and extended wings, as a rule. We attempted to describe them with anisotropic velocity models. When comparing the thermal + microturbulent profile with

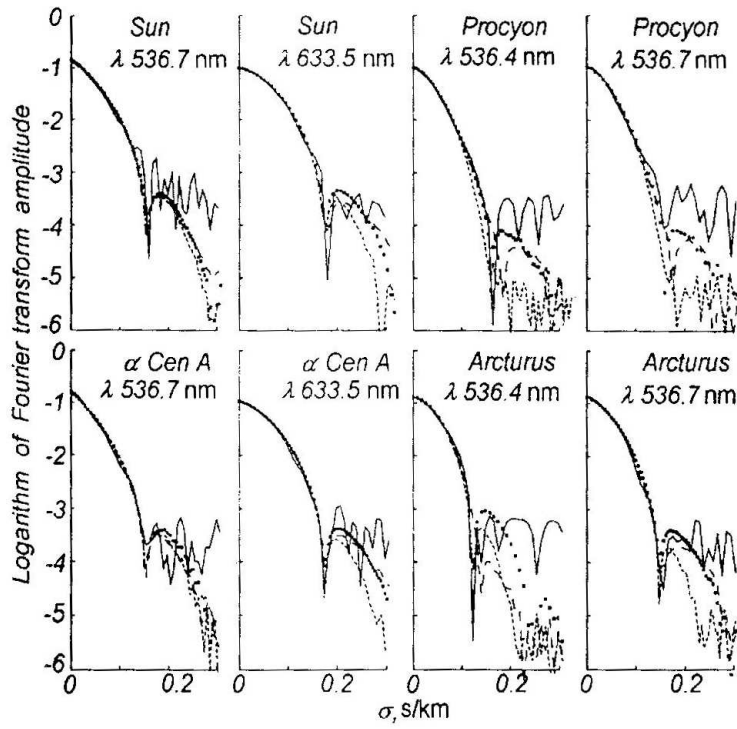


Figure 1: Fourier transforms of the line profiles observed (solid lines) and calculated with different turbulent velocity distributions: isotropic micro-macroturbulent velocities (short dashes); isotropic microturbulence and anisotropic radial-tangential macroturbulence (small squares); anisotropic radial-tangential micro-macroturbulent velocities (long dashes).

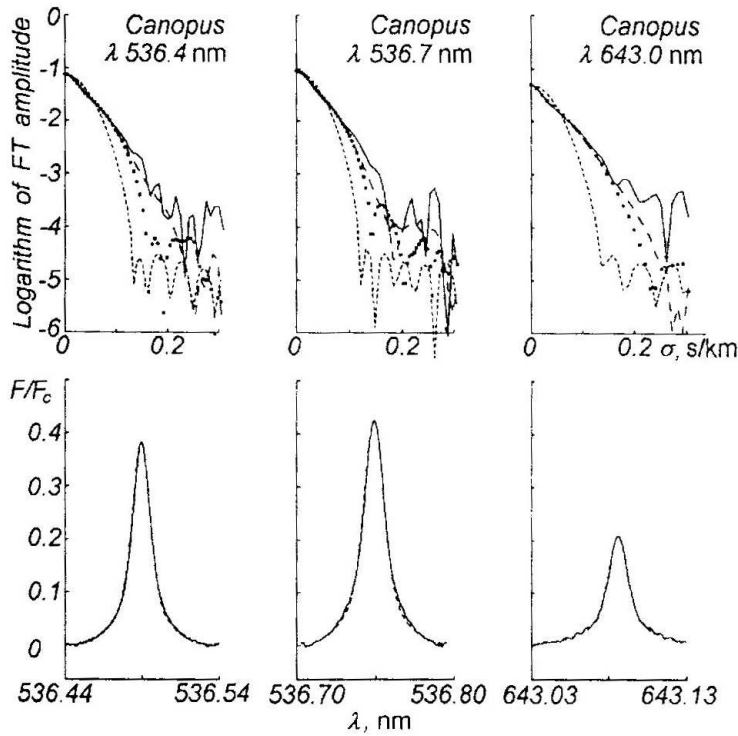


Figure 2: The same as in Fig. 1 for Canopus (upper panel). Given on the lower panel are line profiles for Canopus: observed (solid lines) and calculated (dashed lines).

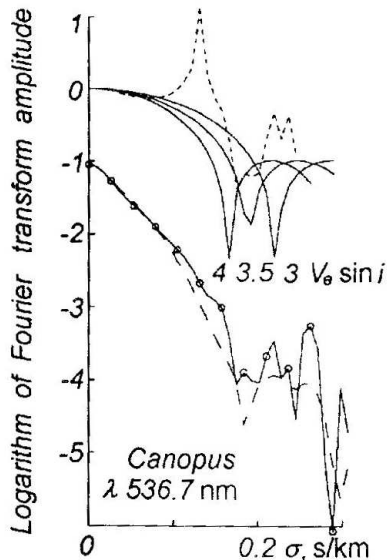


Figure 3: The Fourier transform of the observed line profile $d(\sigma)$ (solid line + circles) and the calculated line profile $f(\sigma)i(\sigma)g(\sigma)$ (long dashes). The Fourier transform of rotation function together with observation noises $g(\sigma)n(\sigma)$ (short dashes) derived from the observed line profile $d(\sigma)$. Solid lines represent the Fourier transforms of the rotation functions calculated with $V_e \sin i = 3, 3.5, 4$ km/s.

observations, we could not determine reliably the microturbulent velocity because the side lobe was greatly distorted by noises and its position could not be fixed exactly. The most adequate value was found to be $V_{mi}^{RT} = 2.1$ km/s. Our calculations suggested that a rotation velocity estimate of 15 km/s derived in [47] was inconsistent with the observed profiles and their Fourier transforms at any microturbulent velocity. For three out of six selected lines ($\lambda\lambda 536.4, 536.7, 643.0$ nm) we could fit the synthesized symmetrical line profiles and Fourier transforms to the observed ones (Fig. 2) only when we adopted 3.5 ± 0.2 km/s for $V_e \sin i$ and the macroturbulence was assumed to have a large radial component (17 ± 2 km/s) and a relatively small tangential component (1.3 ± 1.0 km/s).

The Fourier transforms of rotation functions plotted in Fig. 3 were calculated for $V_e \sin i$ equal to 3, 3.5, and 4 km/s with the limb darkening $\varepsilon = 0.6$; the Fourier transform of the residual observed profile contains the rotation function only (plus measurement noises). It should be noted that the other selected lines, for which we could not choose velocity parameters, are formed higher in the photosphere and they are likely to be affected by the NLTE effects to a greater extent. The velocities derived for Canopus do not defy common sense. Suffice it to look at the profile shape in order to understand that the rotation velocity cannot be too large, otherwise the line cores would be bell-shaped like in the line profiles of Sirius, whose rotation velocity is 15 km/s [10]. The extended wings may be produced by radial high-velocity flows that ascend and then descend without spreading.

So, the microturbulence in cool solar-type stars has an isotropic Gaussian distribution over the stellar disk. The macroturbulence distribution is anisotropic. For hot stars like Canopus a distinct anisotropy is observed in the distributions of micro-macroturbulent velocities. When the macroturbulent velocities determined by different methods and with different approximations (isotropic and anisotropic) are reduced to a common system of *rms* velocities (see V_{rms} in Table 3), the resulting V_{rms} values are in good agreement. This does not hold for Canopus, as V_{ma}^{rad} dominates over V_{ma}^{tan} in it.

5 Errors of the method

Two different models of Arcturus [31] and [36] give the differences $\Delta V_{mi} = 0.2$ km/s in microvelocities and $\Delta V_{ma} = 0.1$ km/s in macrovelocities. For the Sun as a star we obtained $\Delta V_{mi} = -0.1$ km/s and $\Delta V_{ma} = 0.1$ km/s from the models HOLMU [29] and KURUCZ [32]. We may assume, therefore, that the errors due to uncertainties in the parameters of stellar atmospheres are 0.1–0.2 km/s. When the rotation velocity of Arcturus was increased by 0.4 km/s, we got $\Delta V_{mi} = -0.1$ km/s and $\Delta V_{ma} = -0.3$ km/s. The effect of uncertainty in the damping constant is much weaker for Procyon, Arcturus, and Canopus than for the Sun and α Cen A. An increase by a factor of 1.5 in the damping constant gives $\Delta V_{mi} = -0.1$ km/s and $\Delta V_{ma} = -0.4$ km/s for the Sun. Errors due to the choice of the local continuum are also possible. When the continuum for the λ 536.7 nm line in the spectrum of Arcturus is drawn 1 percent higher, the principal lobe in the Fourier transform becomes less steep at higher frequencies and the micro-macrovelocities diminish by 0.1 and 0.3 km/s. Finally, the velocities found from different lines (for all stars except Canopus) differ by 0.2 km/s on the average (Table 3). The difference is due to the fact that the lines form at different heights as well as to noises in the side lobe in the Fourier transforms of the observed profiles.

6 Discussion

Table 4 gives final results for the stars studied.

Microturbulence varies nonmonotonically with effective temperature. It is minimum for the Sun and α Cen A and grows with decreasing and increasing T_{eff} . Such a behavior of microturbulent velocities is well known [18].

The height distribution of V_{mi} is evident from studies [13] and [14]: microturbulence decreases with height only in the atmospheres of the Sun and α Cen A. In Canopus and Arcturus it increases with height in the atmosphere, which is in good agreement with the results of other authors [18]. The behavior of V_{mi} with depth is peculiar in Canopus [4, 13]: it drastically increases with height, and the values derived from the lines of neutral and ionized iron differ considerably. These peculiarities are typical of F supergiants [35]. The simplest isotropic microturbulence model proved to be adequate for all stars except Canopus; the anisotropic model was used for that star.

Macroturbulence also varies nonmonotonically with T_{eff} . The velocity V_{ma} is minimum for G stars. This is in conformity with studies [20, 25], where the temperature dependence of granulation velocities was determined separately for stars of luminosity classes III and IV–V. The depth dependence was determined reliably for the Sun in our studies [14, 28] — macro-turbulence decreases with height in the photosphere. Takeda [46] confirmed this fact from his analysis of a large number of lines by the new method of multiparametric fit of line profiles. The same behavior is displayed by V_{ma} in the photosphere of Procyon [14].

The isotropic macroturbulence model was found to be quite adequate for the Sun and α Cen A. Much better results are obtained for Arcturus and Procyon with the anisotropic model with similar radial and tangential macrovelocity components. A special variant of the anisotropic macroturbulence model with a sharp asymmetry between the radial and tangential components was used for the supergiant Canopus. In general, the anisotropic macroturbulence model may be considered as preferable, since it is adequate for all stars.

The results obtained for the photospheric velocity field in Procyon, Sun, α Cen A, and Arcturus are in accord with the estimates derived from line asymmetries [20, 25]; they are likely to reflect distinctions in the behavior of the photospheric overshooting convection in the

Table 4: Velocity field parameters for five stars from the data of various authors. Type of micro-macro turbulent velocity model is indicated in the last column

V_{mi} , km/s	V_{ma} , km/s	Reference	Note
Sun			
0.5±0.1	3.1±0.1	[16]	$V_{mi}, V_{ma}^{RT}, 5 < W < 15$ pm, Fourier analysis
–	3.8±0.2	[16]	$V_{ma}^{RT}, W < 5$ pm, Fourier analysis
1.2	2.3	[41]	$V_{mi}, V_{ma}, 6 < W < 9$ pm
1.08–0.5	1.92–1.46	[14]	$V_{mi}, V_{ma}, H = 150–300$ km
1.11–1.09	–	[13]	$V_{mi}, \log \tau_5 = -1.71 \div -3.17$
0.5±0.2	2.3±0.4	[46]	$V_{mi}, V_{ma}^{RT}, 10 < W < 20$ pm
–	4.0	[46]	$V_{ma}^{RT}, W < 10$ pm
0.8±0.1	2.6±0.3	Present study	$V_{mi}, V_{ma}, \log \tau_5 = -1.9 \pm 0.2$
a Cen A			
1.54±0.08	–	[44]	$V_{mi}, \text{Ca I}$
1.5–1.06	–	[13]	$V_{mi}, \log \tau_5 = -1.78 \div -2.94$
0.8±0.2	2.9±0.4	Present study	$V_{mi}, V_{ma}^{RT}, \log \tau_5 = -2.3 \pm 0.4$
Procyon			
–	7±0.1	[19]	$V_{ma}^{RT}, \text{Fourier analysis}$
2.1±0.3	4.2±0.5	[45]	V_{mi}, V_{ma}
1.6–1.9	4.1–3.6	[14]	$V_{mi}, V_{ma}, H = 500–900$ km
0.8±0.3	5.9±0.2	Present study	$V_{mi}, V_{ma}^{RT}, \log \tau_5 = -1.8 \pm 0.2$
Arcturus			
1.9	2.5–3.5	[43]	$V_{mi}, V_{ma}^{RT}, \text{Fourier analysis}$
1.7	4.6	[23]	$V_{mi}, V_{ma}^{RT}, \text{Fourier analysis}$
1.8	4.8–5.2	[21]	$V_{mi}, V_{ma}^{RT}, \text{Fourier analysis}$
1.68–1.87	–	[13]	$V_{mi}, \log \tau_5 = -1.55 \div -2.68$
1.0±0.2	4.6±0.3	Present study	$V_{mi}, V_{ma}^{RT}, \log \tau_5 = -1.7 \pm 0.1$
Canopus			
4.5	–	[4]	$V_{mi}, 1 > W > 30$ pm, Fe I
6.0	–	[4]	$V_{mi}, 1 > W > 30$ pm, Fe II, Ti II, Cr II
2.0–4.3	–	[13]	$V_{mi}, \log \tau_5 = -1.4 \div -2.5$, Fe I
2.4–5.4	–	[13]	$V_{mi}, \log \tau_5 = -1.3 \div -2.7$, Fe II
2.1	17–1.3	Present study	$V_{mi}^{RT}, V_{ma}^{rad} - V_{ma}^{tan}, \log \tau_5 = -1.4 \pm 0.1$

main sequence stars and stars on the giant branch [39]. We discuss below some special features of these distinctions.

The Sun as a star. We emphasize a good agreement between our results and the data of other authors (Table 4).

One can see from the radial and tangential microturbulence components determined from the observed center-to-limb broadening of spectral lines [14, 28, 42] that the horizontal micro-velocity is systematically higher by 1 km/s than the vertical one and this difference changes slightly with height. This is confirmed qualitatively by direct stratospheric observations of solar granulation [37]. Thus, the center-to-limb observations of line broadening do not suggest that the microturbulent velocity is isotropic in the solar photosphere. We can use, nevertheless, the isotropic model for the Sun as a star along with the anisotropic model because the relative contribution from the limb regions decreases and the ratio between the tangential and radial components is nearly constant. It is obvious that such an isotropic microvelocity should be considered as some effective quantity.

It follows from the analysis of line profiles [14, 28, 42] and the direct estimates of *rms* velocities from Doppler line shifts in the granulation field [37] that the anisotropy between the horizontal and vertical velocities (the predominance of horizontal velocities) is well defined in large-scale structures; it is reproduced in 2D and 3D solar granulation models [2]. Stratospheric

observations [37] indicate that the anisotropy is much stronger for the large-scale structures ($L > 3.7'' \approx 2700$ km) than for the small-scale ones in the lower and middle photosphere. This may be the cause why the radial-tangential model of macrovelocities differs essentially from the isotropic model and is more adequate for the observed profiles.

The behavior of the parameters found for the photospheric velocity field reflects a decrease of overshooting convection velocities as the predominant process, with oscillatory motions being the governing factor. Multidimensional hydrodynamic simulations and observations of granulation with high spatial resolution [2, 30] suggest that the lower and middle photosphere regions, where most photospheric lines are formed, are controlled by overshooting convection, while oscillatory motions become predominant near the temperature minimum and above it.

α Centauri A. The star is very similar to the Sun in most parameters, but its radius is larger by 23 percent and the mass by 8.5 percent. The gravitational acceleration is smaller by 29 percent than on the Sun (Table 1). The abundances of heavy elements are higher by 0.1–0.3 dex in α Cen A [12, 13, 44], The microturbulent velocity diminishes with height [13], similar to the Sun, but the amplitudes of micro-macroturbulent velocities are larger (Tables 3 and 4). We may assume that higher amplitudes are related to the above-mentioned peculiarities. Indeed, it follows from 3D HD models [39] that the convection velocities, and the atmospheric horizontal flow velocities in the first place, increase with diminishing gravitational accelerations in stellar convective envelopes and atmospheres. The reason is that the pressure and density height scales grow with decreasing g . This results in a growth of the horizontal size of inhomogeneities, since this size is proportional to the density height scale; the horizontal flow velocities increase as well, as it follows from the condition of conservation of mass. The second effect which enhances the vertical and horizontal velocities is a decrease in density and with it in the viscosity of the medium. The third factor is an elevated metallicity, which results in an elevated electron density in the lower photosphere and in an enhanced opacity, as the main opacity source in the continuum is the negative H^- ions, their concentration being proportional to electron density.

Procyon has an effective temperature 700–750 K higher than that of the Sun and a gravitational acceleration 60 percent lower. The radiation dynamics conditions in the upper layers of the star were studied in detail in [2] and [39] based on 3D models. Their major peculiarity is that the thermal convection on Procyon, as distinct from the Sun, makes its way into photospheric layers, since the major supplier of free electrons in the lower photospheric layers on Procyon, due to their higher temperature, is the hydrogen abundant there. As a result, the H^- opacity is much greater, it is extremely sensitive to temperature variations, thus maintaining adiabatic conditions for flows in photospheric layers. The artificial granulation displays, therefore, brightness fluctuations stronger than on the Sun, their growth toward the limb, and a limb effect inverse to the solar one [2]. Macrovelocities on Procyon are by a factor of 2–3 higher than on the Sun, the cause being the same as for α Cen A; they are higher also due to the fact that convective flows have to transport larger energy fluxes.

Arcturus is a red metal-poor giant with low-temperature, low-density atmospheric layers. Considering the results of 3D simulations of stellar granulation on α Cen B [39], which has T_{eff} lower by 600 K than on the Sun, we may assume that the overshooting convection on Arcturus is shifted to deeper layers and manifests itself primarily via velocity field. One more peculiarity is that the size of inhomogeneities is comparable to the star radius (up to 10 percent of R_*) owing to large height scales of density and pressure. Therefore, no more than several “granules” can be found simultaneously on the entire apparent disk of the star. The velocities found by us for Arcturus are higher than on the Sun (Table 3). At the same time, the semiempirical four-component model by Dravins [9], which was specially built for the interpretation of observed bisectors, gives velocities slightly lower than on the Sun. These discrepancies seem to be due to the contribution from oscillations, which we partially detect when analyzing spectral lines.

Canopus is a hot F supergiant distinctive in that its outer layers are in radiative equilibrium. This is the cause for the nonstandard results obtained for V_{ma}^{RT} – a high amplitude of the vertical component with no appreciable horizontal component. Similar solutions were derived from the semiempirical four-component model of Canopus [9] and the analysis of bisectors for the supergiant γ Cygni [26]. A common peculiarity in the line asymmetry in the stars of this type is that it is inverse with respect to the classical line profiles observed in stars with convection-induced photospheric flows. De Jager [6] assumed that such a pattern of the large-scale velocity field in supergiant atmospheres is conditioned by gravity waves.

7 Conclusion

The isotropic distribution of microturbulent velocities and the radial-tangential distribution of macroturbulent velocities seem to represent most adequately the velocity field in the atmospheres of the Sun, α Cen A, Procyon, and Arcturus within the scope of their homogeneous models. For Canopus, the microturbulence is anisotropic and the macroturbulence displays a pronounced asymmetry between its radial and tangential components. The rotation velocity found by us for Canopus turned out to be low.

Acknowledgements. We thank Prof. D. Dravins for furnishing the observational data. The study was partially financed by the State Fundamental Research Foundation of Ukraine (Grant No. 6.4/192).

References

- [1] C. W. Allen. *Astrophysical Quantities* [Russian translation], Mir, Moscow, 1977.
- [2] I. N. Atroshchenko, A. S. Gadun. Three-dimensional hydrodynamic models of solar granulation and their application to a spectral analysis problem, *Astron. and Astrophys.*, vol. 291, no. 2, pp. 635-656, 1994.
- [3] T. R. Ayres, J. L. Linsky, A. W. Rodgers, R. L. Kurucz. Stellar model chromospheres. V. Alpha Centauri A (G2 V) and Alpha Centauri B (K1 V), *Astrophys. J.*, vol. 210, no. 1, pp. 199-210, 1976.
- [4] A. A. Boyarchuk, L. S. Lyubimkov. The atmosphere of Canopus. I. Model atmosphere and microturbulence distribution, *Astrofizika*, vol. 18, no. 3, pp. 375-385, 1982.
- [5] D. H. Bruning. The applicability of the Fourier convolution theorem to the analysis of late-type stellar spectra, *Astrophys. J.*, vol. 281, no. 2, pp. 830-838, 1984.
- [6] C. De Jager. An explanation of the granulation boundary* in the HR diagram, *Solar Phys.*, vol. 126, no. 1, pp. 201-205, 1990.
- [7] P. Demarque, D. B. Guenther, W. F. van Altena. The case of α Centauri: mass, age and p-mode oscillation spectrum, *Astrophys. J.*, vol. 300, no. 2, pp. 773-778, 1986.
- [8] D. Dravins. Stellar granulation. II. Stellar photospheric line asymmetries, *Astron. and Astrophys.*, vol. 172, no. 1/2, pp. 211-224, 1987.

- [9] D. Dravins. Stellar granulation. VI. Four-component models and non-solar-type stars, *Astron. and Astrophys.*, vol. 228, no. 1, pp. 218-230, 1990.
- [10] D. Dravins, L. Lindegren, U. Torkelsson. The rotationally broadened line profiles of Sirius, *Astron. and Astrophys.*, vol. 237, no. 1, pp. 137-147, 1990.
- [11] D. Dravins, Å. Nordlund. Solar granulation. V. Synthetic spectral lines in disk-integrated starlight, *Astron. and Astrophys.*, vol. 228, no. 1, pp. 203-217, 1990.
- [12] I. Furenlied and T. Meylon. An abundance analysis of α Centauri A, *α Astrophys. J.*, vol. 350, no. 2, pp. 827-838, 1990.
- [13] A. S. Gadun. Iron abundance and microturbulence in Arcturus, Canopus, α Cen A, and Sun from Fe I and Fe II lines, *Astron. Nachr.*, vol. 6, no. 1, pp. 413-418, 1994.
- [14] A. S. Gadun, R. I. Kostyk. Analysis of absorption line profiles in the spectra of the Sun and Procyon: velocity field and size of inhomogeneities, *Astron. Zhurn.*, vol. 67, no. 6, pp. 520-527, 1990.
- [15] A. S. Gadun, V. A. Sheminova. SPANSAT: Program for Calculating the LTE Absorption Line Profiles in Stellar Atmospheres, Kyiv, 1988, Inst. of Theor. Phys., Academy of Sciences of UkrSSR, Preprint No. ITF-88-87P.
- [16] D. F. Gray. A test of the micro-macroturbulence model on the solar flux spectrum, *Astrophys. J.*, vol. 218, no. 2, pp. 530-538, 1977.
- [17] D. F. Gray. Turbulence in stellar atmospheres, *Solar Phys.*, vol. 59, no. 2, pp. 193-236, 1978.
- [18] D. F. Gray. The Observation and Analysis of Stellar Photospheres [Russian translation], Mir, Moscow, 1980.
- [19] D. F. Gray. A Fourier analysis of the spectral lines of Procyon, *Astrophys. J.*, vol. 251, no. 1, pp. 152-154, 1981.
- [20] D. F. Gray. Observations of spectral line asymmetries and convective velocities in F, G, and K stars, *Astrophys. J.*, vol. 255, no. 1, pp. 200-209, 1982.
- [21] D. F. Gray. The temperature dependence of rotation and turbulence in giant stars, *Astrophys. J.*, vol. 262, no. 2, pp. 682-699, 1982.
- [22] D. F. Gray. The buying power of high signal-to-noise ratios in spectroscopy, in: *The Impact of Very High S/N Spectroscopy on Stellar Physics*, G. Cayrel de Strobel and M. Spite (Editors), pp. 185-191, 1988.
- [23] D. F. Gray and B. E. Martin. A comparison of turbulence in normal and super-metal-rich K giant stars, *Astrophys. J.*, vol. 231, no. 1, pp. 139-143, 1979.
- [24] D. F. Gray, T. Nagel. The granulation boundary in the H-R diagram, *Astrophys. J.*, vol. 341, no. 1, pp. 421-426, 1989.
- [25] D. F. Gray, C. Toner. Inferred properties of stellar granulation, *Publs Astron. Soc. Pacif.*, vol. 97, no. 592, pp. 543-550, 1985.

- [26] D. F. Gray, C. Toner. The remarkable spectral line asymmetries of F and G Ib supergiant stars, *Publ. Astron. Soc. Pacif.*, vol. 98, no. 603, pp. 499-503, 1986.
- [27] E. A. Gurtovenko, R. I. Kostyk. The Fraunhofer Spectrum and System of Solar Oscillator Strengths [in Russian], *Naukova Dumka*, Kyiv, 1989.
- [28] E. A. Gurlovenko, V. A. Sheminova. Crossing method for studying the turbulence in solar and stellar atmospheres, *Solar Phys.*, vol. 106, no. 2, pp. 237-247, 1986.
- [29] H. Holweger, E. A. Müller. The photospheric barium spectrum: solar abundance and collision broadening of Ba II lines by hydrogen, *Solar Phys.*, vol. 39, no. 1, pp. 19-30, 1974.
- [30] V. N. Karpinsky. Properties of the solar granulation, in: *Solar Photosphere: Structure, Convection and Magnetic Fields: Proc. IAU Symp. No. 138*, J. O. Stenflo (Editor), pp. 67-79, Kluwer, Dordrecht, 1990.
- [31] T. Kipper, M. Kipper, J. Sitska. Some basic parameters of Arcturus including the effective temperature, the surface gravity, and the abundance of some elements are derived, *Tartu Astrofiiis. Obs. Teated*, no. 64, pp. 3-14, 1981.
- [32] R. L. Kurucz. ATLAS: A Computer Program for Calculating Model Stellar Atmospheres, Cambridge, 1970 (SAO Special Report, no. 309).
- [33] R. L. Kurucz. Model atmospheres for G, F, A, B, and 0 stars, *Astrophys. J. Suppl. Ser.*, vol. 40, no. 1, pp. 1-340, 1979.
- [34] L. S. Lyubimkov and A. A. Boyarchuk, "The atmosphere of Canopus. II. Abundances. Determination of the mass, radius, luminosity, and age," *Astrofizika*, vol. 18, no. 4, pp. 596-607, 1982.
- [35] L. S. Lyubimkov, A. A. Boyarchuk. Effects of deviations from LTE on the determination of microturbulence in the atmospheres of F supergiants, *ibid.*, vol. 19, no. 4, pp. 683-696, 1983.
- [36] R. Mäcke, H. Holweger, R. Griffin, R. Griffin. A model-atmosphere analysis of the spectrum of Arcturus, *Astron. and Astrophys.*, vol. 38, no. 1, pp. 239-257, 1975.
- [37] W. Mattig, J. P. Mehlretter, A. Nesis. Granular-size horizontal velocities in the solar atmosphere, *Astron. and Astrophys.*, vol. 96, no. 1/2, pp. 96-101, 1981.
- [38] Å. Nordlund. Modelling of small-scale dynamical processes: convection and wave generation, in: *Small-Scale Dynamical Processes in Quiet Stellar Atmospheres*, S. L. Keil (Editor), pp. 181-221, Sac. Peak Observatory, Sunspot, 1984.
- [39] Å. Nordlund, D. Dravins. Solar granulation. III. Hydrodynamic model atmospheres, *Astron. and Astrophys.*, vol. 228, no. 1, pp. 155-183, 1990.
- [40] S. E. Reynolds, J. B. Hearnshaw, P. L. Cottrell. The spectrum of Canopus - III. Abundances of r- and s-process elements, *Mon. Notic. Roy. Astron. Soc.*, vol. 235, no. 4, pp. 1423-1438, 1988.
- [41] V. A. Sheminova. Turbulence in the photosphere of the Sun as a star. III. Micro/macroturbulence, *Solnech. Dannye*, no. 7, pp. 70-77, 1984.

- [42] V. A. Sheminova. Macro/microturbulence in the solar photosphere, *Kinematika i Fizika Nebes. Tel* [Kinematics and Physics of Celestial Bodies], vol. 1, no. 2, pp. 50-52, 1985.
- [43] M. A. Smith and J. F. Dominy. The dependence of macroturbulence on luminosity in early K-type stars, *Astrophys. J.*, vol. 231, no. 2, pp. 477-490, 1979.
- [44] G. Smith, B. Edvardsson, and U. Frisk. Non-resonance lines of neutral calcium in the spectra of the α Centauri binary system, *Astron. and Astrophys.*, vol. 165, no. 1/2, pp. 126-134, 1986.
- [45] M. Steffen. A model atmosphere analysis of the F5 IV-V subgiant Procyon, *Astron. and Astrophys. Suppl. Scr.*, vol. 59, no. 3, pp. 403-427, 1985.
- [46] Y. Takeda. Analyses of line profiles in the solar flux spectrum for determining rotation and micro/macro turbulence, *Publs Astron. Soc. Jap.*, vol. 47, no. 3, pp. 337-354, 1995.
- [47] A. Uesugi, I. Fukuda. Revised Catalogue of Stellar Rotational Velocities, Depart. Astron. Kyoto Univ., Kyoto, 1982.